following form for the surface recession:

$$\dot{m} = a.\alpha_0.f(D)[1 - \beta(\dot{m}_g + \dot{m}_c)/\alpha_0] - \dot{m}_g K_{0_g} + he^{-T_R/T}[\eta dp/ds + \psi_1\tau(1 + l\psi_2\tau + ..) + Kp_e(1 + K'p_e + ..) - n\dot{m}_g/p_e] \quad (9)$$

For the sets of measurements concerning relatively low wall temperature, where combustion is limited by the kinetic reaction rather than by the diffusion reaction, these sets agree with the other provided that values assumed for the following parameter are appropriate:

D = kinetic recession rate/diffusion recession rate = $\frac{4}{3}K_v p_e^{1/2} e^{-T_{ox}/T} K_{0_e}^{1/2}/\alpha_0 \psi K_{0_e}$

or

$$D = K_1(p_e^{1/2}/\alpha_0)e^{-T_{ox}/T} \quad (10)$$

and we introduce in Eq. (8) following Scala[9] and Medford[4]

$$f(D) = (D/2)[(D^2 + 4)^{1/2} - D] \quad (11)$$

and ψ_1 as a blocking factor for τ.

The test runs enabling the various parameters of Eq. (8) to be determined—a phenomenological determination being alone possible—were under way at Aerospatiale Oct. 15, 1970. The initial results are submitted in the following paragraph.

Experimental Results

We have so far conducted simulations in a 1500-kw plasma-jet facility. They provided sets of values to τ, p_e, α, that stem directly from experimental measurements, except for τ, which is calculated.

These initial experimental results are compared, in Table 1, with theoretical results obtained with a simplified form of Eq. (9) as follows:

$$\dot{m}_{calc} = \rho s = a\,\alpha\,(D/2)[(D^2 + 4)^{1/2} - D] + he^{-T_R/T}(\tau + Kp_e) \quad (12)$$

Relation (12) is deduced from Eq. (9) by assuming $\eta = 0$, $l = 0$, $n = 0$, and $K_{0_g} = 0$. We next determine by a least-squares method

$$a = 0.1516,\ h = 9.318\ 10^{11}\ (1/\text{sec}),\ K = 5.461\ 10^{-3}$$

$$T_R = 60000°\text{K},\ T_{ox} = 27500°\text{K};\ K_1 = 4500$$

The differences of $\dot{m}_{calc}$ from the measured $\dot{m}_{exp}$ are satisfactorily small. As a matter of fact, the mean error is ~10%, and it may be considered that calculation of ablation rate to within 20% is satisfactory.

In conclusion, for over-all erosion rate calculation (mechanical + thermochemical), good results, in relation with local environmental conditions, are obtained from a simple phenomenological expression. In this expression, the thermochemical coupling with the boundary layer is a close approximation, but can be entirely calculated in diffusion state, thereby allowing a direct determination of mechanical erosion. The results are already satisfactory and can be easily improved, especially if the pressure longitudinal gradient is taken into account.

References

[1] Bethe, A. and Adams, M., "A Theory for the Ablation of Glassy Materials," *Journal of the Aerospace Sciences*, Vol. 26, No. 6, 1959, p. 321.

[2] Poch, W. and Dietzel, A., "Die Bildung von Silizum Karbid aus Silizum Dioxyd and Kohlenstoff," *Deutschen Keremischen Gesellschaft*, Vol. 39, No. 8, 1962.

[3] Munson, T. R. and Spindler, R. J., "Transient Thermal Behaviour of Decomposing Materials," IAS Paper 62-30, 1962.

[4] Medford, J. E., "Development and Application of a New Approach to Heat Shield Thermal Design and Evaluation," AIAA Paper 62-259, Washington, D. C., 1964.

[5] Schneider, P. J., Dolton, T. A., and Reed, G. W., "Mechanical Erosion of Charring Ablators in Ground Test and Re-Entry Environment," *AIAA Journal*, Vol. 6, No. 1, Jan. 1968, pp. 64–72.

[6] Bishop, W. M. and di Cristina, V., "A Prediction Technique for Ablative Material Performance under High Shear Re-Entry Conditions," *AIAA Journal*, Vol. 6, No. 1, Jan. 1968, p. 59.

[7] Kendall, R. M. et al., "An Analysis of the Coupled Chemically Reacting Boundary Layer and Charring Ablator," CR 1061 at 1065, 1968, NASA.

[8] Bartlett, E. D., Anderson, L. W. and Curry, D. M., "An Evaluation of Ablation Mechanisms for the Apollo Heat Shield Material," *Journal of Spacecraft and Rockets*, Vol. 8, No. 5, May 1971, pp. 462–468.

[9] Gilbert, L. M. and Scala, S. M., "Heterogeneous Combustion and Sublimation of Cones, Spheres and Wedges at Hypersonic Speeds," *AIAA Journal*, Vol. 3, No. 11, Nov. 1965, pp. 2124–2131.

Optical Technique for the Measurement of Local Velocities in Single- and Two-Phase Flowfields

R. J. Burick,* G. L. Cline,† and R. N. Gurnitz‡
Rocketdyne, Division of North American Rockwell Corp. Canoga Park, Calif.

In dense two-phase flowfields, neither Pitot-tube nor hot-wire probes work with any degree of success. For local particle velocity measurements, streak and high-speed-framing photography have been used, but the data reduction is laborious and often subject to reading errors. This Note presents a crossed-beam optical technique that has been used to measure local gas velocities in a gaseous N_2 freejet and local droplet velocities in a dense gas/liquid sprayfield. For the latter, a gas/liquid rocket-motor injector element was used with water and N_2 as nonreactive propellant simulants. Local liquid/gas mass flow ratios up to ~10 and droplet number densities up to ~10^9/ft^3 were employed.

Approach and Apparatus

Two reference points in the flowfield are provided by two focused beams spaced ΔX (~0.1 in.) apart (Fig. 1). The intensity fluctuations of the focused light beams are monitored by two photodetectors (Fig. 2), and local values of velocity

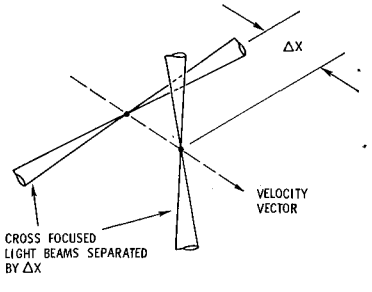

Fig. 1 Perspective drawing of crossed focused beams.

Presented as Paper 70-728 at the AIAA Reacting Turbulent Flows Conference, San Diego, Calif., June 17–18, 1970; submitted September 10, 1970; revision received February 19, 1971. The authors are indebted to William Herget, Rocketdyne, for his assistance in the design of the crossed-beam optical system, to Edward Drolinger, Princeton Applied Research, Anaheim, Calif., for supplying on loan the real-time cross-correlation computer, and to D. E. Zwald for assisting in the experimental studies.

* Member of the Technical Staff, Advanced Programs. Member AIAA.

† Member of the Technical Staff, Advanced Programs, presently with Autonetics, Anaheim, Calif.

‡ Manager, Exploratory Engineering, Advanced Programs.

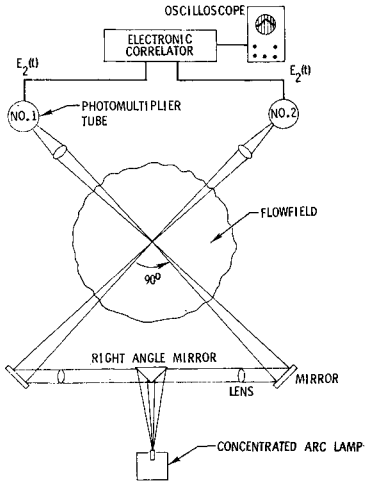

Fig. 2 Crossed-beam optical system viewed in a plane normal to the flowfield velocity vector.

are determined from

$$V = \Delta X/\tau_{\text{transit}} \tag{1}$$

where τ_{transit} is the mean transit time (determined electronically by a cross-correlation technique) of fluid or particles between the reference points. In single-phase gaseous flows, an optically absorbing tracer gas is fed continuously into the flowfield. Because of the macroscopic turbulent structure of the flowfield, local tracer gas densities are established and conserved for short distances (~0.10 in.) as confirmed by the high-speed filming of an N_2 freejet flowfield using ~2% by weight of NO_2 as the tracer gas. The density gradients due to the tracer gas result in corresponding fluctuations in the intensities of the focused light beams. In two-phase flows, droplet density and size are conserved for short distances (~0.10 in.) in the flowfield, as confirmed by high-speed motion picture data discussed later.

The mean transit time is determined by cross-correlation of the outputs of the two photodetectors, whose real-time characteristic outputs are shown in idealized form in Fig. 3. These two outputs, $E_1(t)$ and $E_2(t + \tau_{\text{transit}})$ are similar due to the conservation of the macrostructure of the tracer gas or droplet flowfields. They are displaced in time by τ_{transit}. The cross-correlation function[1]

$$G(\tau) = \underset{T\to\infty}{\text{Limit}} \frac{1}{2T} \int_{-T}^{T} E_1(\tau)\, E_2(t + \tau)dt \tag{2}$$

describes the degree of conformity between E_1 and E_2 as a function of their mutual delay τ; $G(\tau)$ displays a maximum when the displacement time between the two signals τ is equal to τ_{transit} (lower portion of Fig. 4).

To achieve satisfactory spatial resolution the experimental system utilized a crossed-beam configuration. (Figure 1 is a simplified perspective drawing of the beams near their crossings. If parallel light beams were employed instead of crossed beams, local measurements of velocity would not have been possible even with well focused beams, because some

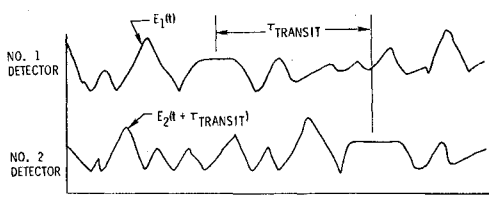

Fig. 3 Determination of τ_{transit}.

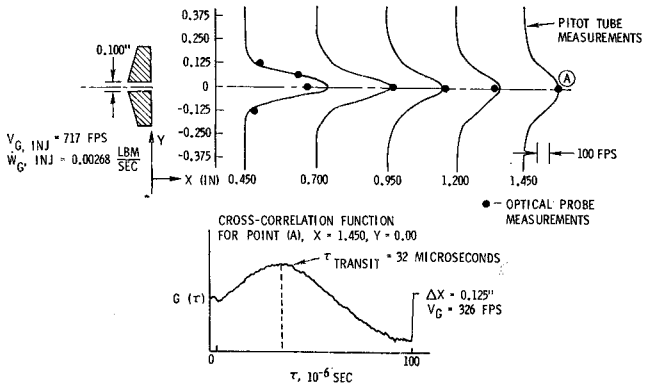

Fig. 4 Single-phase velocity data.

optical averaging of the flow structure would have been unavoidable.) The beams are focused to a diameter of the order of 0.010 in. to ensure that ΔX can be made small. Spatial resolution is achieved by means of this beam configuration, because only the turbulent tracer gas structure or particles that intersect both beams produce a nonzero correlation. Hence, the measurement volume is confined to the region of beam crossing.

In Fig. 2 the light source is a Sylvania 10-w, zirconium-concentrated (0.010-in.-diam) arc lamp with a regulated d.c. power supply containing built-in starting circuitry. A beam splitter, pairs of lenses, and a pair of mirrors are used to generate two perpendicular beams with nearest separation adjustable down to ~0.050 in. A pair of lenses image the beams onto two RCA 1P28 photomultipliers. After amplification, the signals are cross-correlated by a Princeton Applied Research Model 101 Correlation Computer, which simultaneously calculates $G(\tau)$ for 100 different values of τ in real time directly from the photomultiplier analog inputs. The $G(\tau)$, displayed on an oscilloscope, is photographed. It should be noted that correlation of fluctuations due only to the arc lamp (i.e., nonflow modulated) would have resulted only for a value of $\tau_{\text{transit}} = 0$. However, because the light source was essentially ripple-free, correlations for values of $\tau_{\text{transit}} = 0$ were barely detectable.

Single-Phase Velocity Measurements

An N_2 freejet flowfield was generated from a 0.100-in.-diam, sharp-exit orifice having a length/diameter ratio of ~15 and provisions for adding tracer gas (~2% by weight of NO_2) upstream of the orifice entrance. Independent velocity measurements were made with a $\frac{1}{16}$-in.-diam pitot tube (at five axial locations) together with an MKS Baratron electronic pressure meter. As shown in Fig. 4, measurements by the optical velocimeter (points) and pitot tubes (curves) are in essential agreement. Also shown is $G(\tau)$ as generated by the cross-correlation computer for the datum point at $X = 1.45$

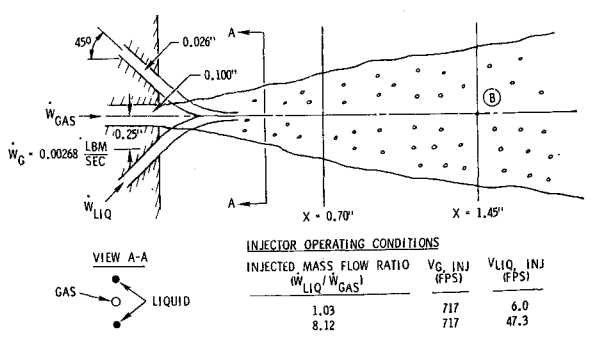

Fig. 5 Gas/liquid injector element.

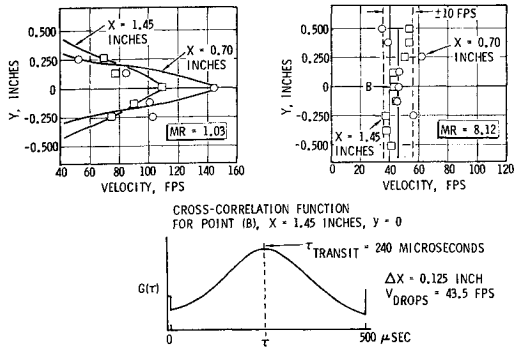

Fig. 6 Droplet velocity data.

in. and $Y = 0$; $\tau_{transit}$ is the τ corresponding to the maximum value of $G(\tau)$. For this case, $\tau_{transit} = 32$ μsec.

Velocity Measurements in Two-Phase Flows

The center gas jet of the injector element (Fig. 5) was the same orifice that was used for the single-phase experiments. For the two-phase experiments, two 0.026-in.-diam, impinging liquid orifices were added, such that the total included impingement angle of the liquid jets was 90° with the theoretical impingement point on the axis of the center gas orifice. Local droplet velocities were measured at two axial locations with nominal injected mass flowrate ratios ($\dot{w}_{liq}/\dot{w}_{gas}$) of 1 and 8. The mass flowrate of the center gas jet was the same as in the single-phase experiments.

In Fig. 6 the measured droplet velocity profiles at the low mass flow ratio ($MR = 1.03$) are similar to the single-phase ones in Fig. 4. The central gas jet atomizes the two liquid jets and accelerates the droplets as would be expected when the ratio of gas momentum to liquid momentum is high (~100). The highest droplet velocities correspond to the regions where the gas velocity is highest (i.e., near the jet centerline). The droplet velocities decay (as do the gas jet velocities) as they move from $X = 0.7$ to $X = 1.45$ in. In contrast, for $MR = 8.12$ in Fig. 6, the droplet velocity profiles show little variation with either axial distance or radial position, because when the gas/liquid momentum ratio is low (~1), the liquid jets, behaving almost independent of the gas jet, atomize and assume axial velocities that approximate the liquid injection velocities. Figure 6 also presents $G(\tau)$ for point B ($X = 1.45$ in., $Y = 0$), where $\tau_{transit} = 240$ μsec and $\Delta X = 0.125$ in., so that the mean droplet velocity was 43.5 fps.

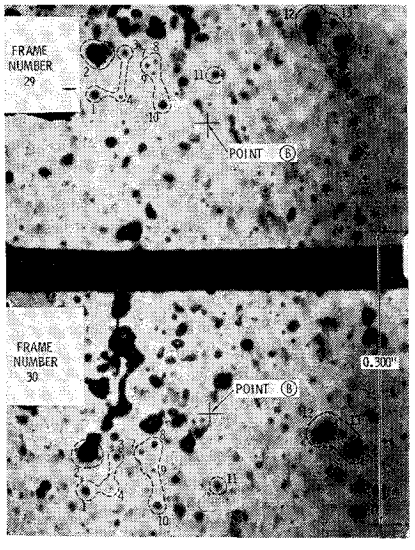

Fig. 7 Successive frames from high-speed film.

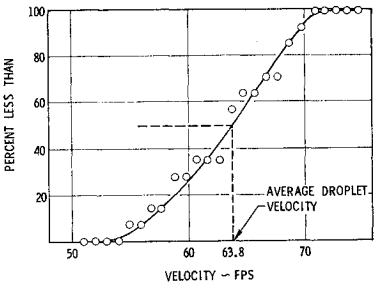

Fig. 8 High-speed film droplet velocity data.

Independent measurements of droplet velocities were made at point B (Fig. 5) by photographing the sprayfield ($MR = 8.12$) with a Fastax camera operated at 7132 frames/sec as determined from images from a 1000-Hz timing light on the film margin. The sprayfield was backlighted with a xenon strobe light collimated with two lenses. Figure 7 shows locations of 14 droplets (~60 to 600 μ diameters) in two successive frames. The macrostructure of the droplet flowfield is seen to be conserved for short distances. Figure 8 presents the results for 14 droplets. (No correlation between droplet diameter and measured velocity was evident.) The average velocity was 63.8 fps, which is higher than the 43.5 fps nominal value from the optical velocimeter. This discrepancy has not been conclusively resolved but is believed to be due to a systematic measurement error (such as in beam spacing) rather than to an inherent system limitation. During the course of the investigation, adjustments to the beam spacing were made (the system was designed to permit continuous adjustment of the spacing from 0 to ~0.50 in.), and a spacing error of ~0.058 in. would have resulted in the observed discrepancy.

Preliminary attempts were made to measure gas and particle velocities simultaneously, but the $G(\tau)$'s obtained exhibited only maxima corresponding to the particle velocities rather than dual maxima corresponding to both gas and particle velocities. This was not too surprising, since the amplitudes of the photomultiplier tube signals were 10 to 100 times greater for particles than for the NO_2 tracer gas, because a particle traversing the beam attenuates almost 100% of the light, whereas the tracer gas absorbs only a few percent.

To allow for discrimination between the tracer gas and particle signals, a diode clipper circuit was inserted before the input of the correlator. The signal amplification was then increased until signals from both particles and tracer gas were greater than the voltage clipping level. Use of the clipping circuits did not have an effect on the gas velocity measurements that were made in the single-phase flows or on the particle velocity measurements that were made in the two-phase flows. However, still only single maxima in $G(\tau)$ could be obtained, and they corresponded to droplet (rather than gas) velocities.

Concluding Remarks

This study has demonstrated the feasibility of a technique employing a crossed-beam optical system and a correlation computer for noninterference measurement of local gas velocities ($V = \Delta X/\tau$) in single-phase freejet flowfields and particle velocities in two-phase flowfields. However, further work is required for demonstration of simultaneous gas and particle velocity measurements. The technique is expected to be useful for droplet drag studies in reacting and nonreacting turbulent flowfields, two-phase flow mixing studies, reacting gas flow studies, two-phase rocket exhaust studies, and noninterference chemical process flow stream measurements.

Reference

[1] Lee, Y. W., *Statistical Theory of Communication*, Wiley, New York, 1960.